Moore, J. C., Mascle, A., et al., 1990
Proceedings of the Ocean Drilling Program, Scientific Results, Vol. 110

27. ODP LEG 110: TECTONIC AND HYDROLOGIC SYNTHESIS[1]

A. Mascle[2] and J. C. Moore[3]

ABSTRACT

During Leg 110, the northern Barbados Ridge was penetrated at six sites ranging from 6 km seaward to 17 km arcward of the deformation front. Reference Site 672 in the abyssal plain provides a unique record of paleoenvironments prevailing at the latitude of the Caribbean in the western Atlantic. At this site Senonian to lower Pleistocene pelagic and hemipelagic sedimentation was punctuated by (1) locally derived middle Eocene and Oligocene calcareous turbidites, (2) South American derived middle and upper Eocene and Oligocene terrigenous turbidites, and (3) arc-derived Neogene ash falls.

The Neogene section is currently accreting at the deformation front while low-angle thrusts are propagating seaward from the décollement. Balanced cross sections, with corrections for porosity loss, suggest 40% shortening of the Neogene accreted section within 7 km of the deformation front. The underthrust series show little or no deformation, but slightly higher porosities than expected suggest overpressuring. A decrease in the percentage of smectite interlayers in the underthrust sequence suggests diagenetic processes possibly involving neoformation of illite and the release of free water. Possibly underplated, stratally disrupted sediments occur at the sites located furthest uplsope.

Anomalies in temperatures and pore-water geochemistry specify fluid migration pathways including the décollement zone, active thrusts, and Eocene sand layers in the underthrust sequence. Anomalies of probable thermogenic methane in the décollement zone suggest long-distance lateral migration in this conduit. The negative chloride anomalies characteristic of the migration conduits might be generated by smectite dehydration at the fluid source areas. The décollement and thrust faults probably have a cyclic history of variable fluid flow and related variable fluid pressure and permeability, superimposed on a lower background flow rate. This apparent episodic flow is consistent with the model of deformational pumping associated with incremental displacement along faults. However, the décollement could undergo faulting and simultaneous fluid influx, in a steady state, because it can be a surface of minimum head and minimum effective stress, given reasonable pressure gradients.

INTRODUCTION AND REGIONAL SETTING

Leg 110 was devoted to the study of tectonic and hydrologic processes occurring at the toe of the Barbados Ridge, a broad accretionary prism that developed in the Tertiary at the leading edge of the eastward-moving Caribbean Plate (Fig. 1, back pocket). This summary of the geologic and hydrologic results of Leg 110 draws largely on papers in this volume; the reader is referred to previous syntheses (Mascle, Moore et al., 1988 and Moore, Mascle, Taylor, et al., 1988), which focused more specifically on the initial results of the cruise, some of which are not repeated here.

Subduction of Atlantic oceanic crust underneath the accretionary prism and underneath the eastern tip of the Caribbean basement is clearly depicted by a deep seismic profile crossing the entire forearc about 75 km north of the Leg 110 transect (Ladd et al., this volume). As a consequence of subduction, a volcanic arc developed from the earliest Eocene along an arcuate line about 1000 km long running southward from the Venezuelan shelf (Los Testigos island) to the Anegada Passage (Noroit seamount) and northward to the Virgin islands (Bouysse et al., this volume). Accretion at the Barbados Ridge deformation front is expressed by a broad range of tectonic structures that are influenced by sediment thickness and the presence of several transverse basement highs on the incoming Atlantic oceanic crust (Mascle et al., this volume). ODP Leg 110 and DSDP Leg 78A are located on the western tip of one of these highs, the Tiburon Rise (Fig. 1, back pocket). Drilling was done here to avoid deep water depths to the north (with the possibility of strong dissolution of calcareous microfauna and poor biostratigraphic determinations), and excessive sedimentary thicknesses to the south (which would have prevented reaching the oceanic basement).

The collision of the Tiburon Rise at the subduction zone has induced radical changes in the structure of the Lesser Antilles forearc. One major feature is the sharp decrease in volume of incoming sediments from south to north. This effect is expressed by the decreasing volume and increasing water depth of the accretionary prism from south to north. The additonal sediment load to the south increases the basement depth at the deformation front from less than 1 km in the Leg 110 area to more than 11 km at the southern boundary of the subduction zone. Other possible consequences of the subduction of the Tiburon Rise are the closing of the broad Tobago forearc basin to the north and the Pleistocene uplift of the eastern edge of the volcanic arc (expressed by the 200-m uplift of the Pliocene-Pleistocene shallow marine carbonate rocks of La Désirade and Guadeloupe, Bouysse et al., this volume). These variations along the strike of the Lesser Antilles forearc influence not only the regional geology but have to be considered when interpreting the three-dimensional aspects of fluid migration along our single east to west transect.

The Tiburon Rise also induces tectonic features at the deformation front, such as lateral ramps and related anticlines (Fig. 1, back pocket). Apparently the Tiburon Rise does not affect the frontal thrusts in the Leg 110 area, which appear to trend north to south, almost perpendicular to the plate convergence vector. However, we cannot preclude that the out-of-sequence thrusts, developed upslope, have a trend oblique to the frontal thrusts due to the impingement of the Tiburon Rise.

[1] Moore, J. C., Mascle, A., et al., 1990. *Proc. ODP, Sci. Results*, 110: College Station, TX (Ocean Drilling Program).
[2] Institut Français du Pétrole, BP 311, 92506 Rueil-Malmaison cedex, France.
[3] University of California, Santa Cruz, CA 95064, USA.

BIOSTRATIGRAPHY, LITHOLOGY, AND SEDIMENTARY HISTORY

Because of some inconsistencies in ages used in Mascle, Moore, et al. (1988), we have included here (Fig. 2) the most authoritative summary of age zonations from Clark (cenozoic calcareous nannofossils, this volume). The age calls are principally based on nannofossil zonations; however, where the section was barren of calcareous detritus, radiolarians provided critical age information. The relatively slow sedimentation rates and the rich diversity of the tropical fauna and flora in the Leg 110 cores provide a high degree of biostratigraphic resolution. Accordingly, biostratigraphically defined structural features are better resolved here than at any other convergent margin drilled by DSDP or ODP.

The lithologic and biostratigraphic sequence defined on the incoming oceanic plate provides the key to evaluating the structural, diagenetic, and geotechnical evolution of the deformed prism and underthrust sediments (Figs. 2 and 3). A complete sedimentary sequence ranging in age from early Eocene to early Pleistocene has been cored at ODP Site 672. During DSDP Leg 78A the remainder of the section down to oceanic crust was cored at Site 543, located about 20 km north of Site 672 (Biju-Duval, Moore et al., 1984). These two boreholes thus provide a complete and unique record of the paleoenvironments prevailing in the western Atlantic Ocean at the latitude of the Caribbean for most of the Tertiary and the latest Cretaceous (Campanian). This incoming sedimentary sequence is sub-divisible into three main lithologic successions.

The lower succession of the incoming sedimentary sequence (Campanian to early middle Eocene age) represents a pelagic to hemipelagic sedimentation in an open marine environment with carbonate-bearing sediments restricted to the upper Cretaceous section. The lower and lower-middle Eocene clays at Site 672 show large amounts of kaolinite and smectites. We think they originated from soils overlying basic eruptive rocks that develop under equatorial climates (Capet et al., this volume). A similar conclusion was proposed by Latouche and Millet (1984) for the Eocene clays of Site 543. Whether these soils were formed on the South American continent to the south or on the Caribbean island arc to the west has not been determined.

The second lithologic succession of the incoming sedimentary sequence (middle Eocene to Oligocene age) is characterized by the influx of turbiditic layers superimposed on a background of hemipelagic sedimentation (Dolan et al., Beck et al., this volume). This Eocene section shows both calcareous fine-grained turbidites and calcareous siliclastic turbidites. The first were probably redeposited from higher on the Tiburon Rise. The second probably originated from the South American continent. Assuming no drastic changes in the seafloor morphology since Eocene, siliclastic deposits on the Tiburon Rise imply significant upslope flow of turbidity currents in a very distal environment (about 800 km from the continental shelf). The Oligocene section shows predominantly calcareous turbidites and only a small amount of terrigenous silty turbidites.

The most obvious regional correlative of the terrigenous turbidites of Site 672 is the Scotland Group of Barbados Island. The Scotland Group is approximately age equivalent to the Site 672 terrigenous turbidites (Eocene to middle Oligocene); the Scotland Group probably represents distal deepsea fan or trench deposits originating from the northern South American margin (Pudsey et al., 1982; Speed, 1983; Baldwin et al., 1986). These turbidites, however, do not contain the abundant shelf-derived detritus that characterized Site 672 turbidites (Dolan et al., this volume). Such exotic coarse components, including small benthic forams, igneous-metamorphic quartz, and glauconite, are present in the middle Eocene Caratas Formation in northern Venezuela. This distal platform or upper slope facies could therefore represent a proximal equivalent of rocks cored at Site 672. Both are probably related to the erosion of mountains generated by the Eocene-Oligocene climax of tectonic activity in South America. The much smaller amount of terriginous sands and silts in the Oligocene strata, and their complete disappearance in the Neogene sediments, may have resulted from capturing of the source area (Guyana Shield) by a new river system that drained from west to east. (Beck et al., this volume).

The Lesser Antilles volcanic arc was active from the earliest Eocene to early late Oligocene. The lack or scarcity of volcanic ash in the Eocene and Oligocene strata of Site 672 could be explained by the fact that a large number of volcanoes erupted in a submarine environment, so that only a small amount of ash was dispersed by the wind (Bouysse et al, this volume). Some volcanoes, however, produced ash falls, because ash layers occur in the deep marine marls and siliceous clays of Barbados Island (oceanic formation). These rocks were probably deposited at the back or on top of the juvenile accretionary complex closer to the volcanic arc than the sediments at Site 672.

The third and uppermost portion of the incoming sediments is of Neogene age. Pelagic to hemipelagic sedimentation prevailed at that time, with a conspicuous ash layer. The influx of this volcanic ash is particularly well recorded by the magnetic susceptibility of the rocks. Magnetic susceptibility was mainly controlled in Eocene and Oligocene times by paramagnetic minerals such as amphiboles, pyroxenes, and chlorites (from South America); since the middle Miocene the increased susceptibilities have been related to ferromagnetic minerals, such as abundant titanomagnetites from the volcanic ashes (Hounslow, this volume). The rapid increase in ash falls at Site 672 in the early Miocene is clearly correlated with the renewed Neogene activity of the Lesser Antilles volcanic arc (Bouysse, this volume).

The clay mineralogy of the middle Miocene to lower Pleistocene sediments shows a slow but significant increase of illite, chlorite, and kaolinite with respect to the smectites that generally prevailed in Paleogene times. This evolution might be related to some influxes of fine-grained clastics from South America linked to the Orinoco delta system (if all these clays are predominantly primary continental minerals; Capet et al., this volume), and/or to better preservation of volcanic ash in recent time (if smectites were formed by submarine alteration of ash; Schoonmaker Tribble, this volume). This evolution could also reflect a general progressive cooling of the climate and an increasing influence of the Antarctic Bottom Current (AABW) in front of the Lesser Antilles margin (Capet et al., this volume). Shifts in the specific abundances of benthic deep-water foraminifers from early Pliocene to early Pleistocene also support this increasing importance of the AABW (Clark, deep water foraminifers, this volume).

The sedimentary history at Site 672 was thus controlled by a background of pelagic and hemipelagic deposition. Influx of locally derived (Tiburon Rise) calcareous turbidites occurred in middle Eocene to Oligocene with long-distance transport terrigenous turbidites in the middle and late Eocene, and to a lesser extent, Oligocene. Ash falls from the Lesser Antilles volcanic arc were conspicuous in the Neogene. If siliclastic turbidites from South America reached Site 672 during the Eocene, why didn't similar coarse-grained clastic components reach this location during the Pliocene and Pleistocene? Certainly the Orinoco river system was supplying a large terrigenous influx. Perhaps any coarse material being transported by turbiditic or bottom currents moved around the Tiburon Rise to the east rather than to the west due to the eastward growth and movement of the accretionary complex (Brown and Westbrook, 1987). Indeed, fine-

grained turbiditic layers together with sandy and silty clays occur in the few cores of the Neogene section drilled at DSDP Site 27 located about 100 km northeast of the Tiburon Rise.

STRUCTURAL GEOLOGY AND PHYSICAL PROPERTIES

A major objective of Leg 110 was the study of accretionary processes in an area of thin oceanic sedimentary cover (a few hundred meters) and, as a consequence, relatively poor seismic resolution. This is in contrast to the southern edge of the Barbados Ridge where the huge volume of accreted sediments allows excellent seismic control as well as giving a clear picture of seafloor manifestations of thrusts, folds, and mud volcanoes (Brown and Westbrook, 1987; Mascle et al., Faugéres et al., this volume). Our results allow a detailed analysis of large-scale and small-scale structures that developed at the toe of an accretionary complex, thus allowing a direct comparison to be made with older onshore thrust belts (Fig. 4).

Three main tectonic processes acted simultaneously at the leading edge of the accretionary complex: (1) initial offscraping above a décollement at the deformation front, (2) subsequent thickening of the wedge further upslope, and (3) sediment underthrusting below the décollement, possibly followed by underplating in the inner part of the prism.

The overall geometry of initial imbrication by offscraping is relatively clearly established (Fig. 4). However, because the structures are poorly imaged by seismic profiles, several different balanced sections have been proposed (Brown et al., this volume). Imbricate thrusting above a décollement in a lower Miocene stratigraphic layer is the dominant tectonic process across the first 5 km of the wedge, with secondary imbrication in the accreted packets. The resulting amount of shortening across the first five major packets is at least 25%, and could be as great as 35%. When porosity loss is taken into account, a total shortening of about 40% is achieved. The arcward-most and oldest of the five thrusts was emplaced on late Miocene to early Pleistocene mudstones about 0.5 m.y. ago. The present horizontal length of the five packets is close to 7 km. Their initial length was thus about 12 km, and the horizontal shortening is 5 km. The balanced sections thus indicate a shortening rate of 1 cm/yr, about half of the plate-convergent rate proposed by Stein et al. (1987). This, however, remains an approximate estimate because small-scale deformation (microfolds and faults), and surface erosion and syntectonic sedimentation are difficult to assess and have not been taken into account. The remaining shortening is probably distributed over the inner part of the accretionary wedge.

Site 676 is located near the deformation front, only 250 m arcward from the emergence of the frontal thrust. Three faults have been encountered in this single section (Fig. 3). All of these faults show positive anomalies in methane and manganese pore fluid content (Blanc et al. pers. commun.), indicating advection of fluids from the inner part of the prism. The upper thrust at about 40 mbsf is associated with folding of Pleistocene strata above, with bedding dips as steep as 7°; apparently this fault is associated with a zone of macroscopically ductile deformation as the upward propagating thrust reaches the youngest and least-consolidated sediments. The second thrust at 200 mbsf corresponds to a stratigraphic inversion and could represent a new seaward-propagating thrust, whose seafloor emergence is tentatively recognized 2 km seaward from the presently obvious deformation front. The deepest tectonic feature is the décollement, which is documented by both a slight stratigraphic inversion and the presence of an horizontal array of sigmoidal subvertical veins (as at Site 672, 6 km seaward from the deformation front and in the same stratigraphic interval).

Following the model of Cello and Nur (1988) we propose that tectonic loading resulting from thrusting at the deformation front induced the development of high pore pressure in the foreland. The correlative reduction of shear strength in the sediments was probably greater in stratigraphic layers with high initial water content, such as the early Miocene interval (Wilkens et al, this volume) where the décollement is located. Because the Neogene sediments have a high overall water content (between 35 and 60% total weight), their shear strength is probably uniformly low relative to the underthrust sediments. The Neogene sediments are therefore "bulldozed" off the underthrust sequence, leading to the simultaneous propagation of several active thrusts branching off from the décollement.

There is an apparent thickening of the décollement zone from the abyssal plain (where it appears as a 20-m-thick incipient shear zone) to the inner part of the prism where at Site 671 it encompasses a 40 to 50-meter-thick section with a well-developed scaly fabric (Brown et al., this volume). This scaly fabric could represent original discrete shear surfaces, as most of them are polished and striated. Well-developed foliation with striations is clear in radiolarian-bearing samples of the décollement zone (Y. Ogawa, pers. commun.). This fabric, however, is not obvious in the microfabric of the rocks, as backscatter SEM imagery of sediments from the décollement at Site 671 has not revealed any preferential orientation of clay minerals (Prior et al., this volume).

The accretionary prism thickens from about 300 m at Site 676 to about 2 km beneath Site 674. Three main tectonic processes cause this thickening (Brown et al. (1), this volume): (1) backrotation and folding of the initial accreted packets, (2) out-of-sequence thrusts, and (3) underplating. Correlative to thickening is an increase in the volume of rocks affected by the scaly fabric and disrupted zones. Calcite veining becomes important, with its first occurrence in the accretionary prism at Site 673, and an incipient axial plane cleavage indicative of pure shear strain begins to develop at Site 674, i.e., only 18 km from the deformation front. Such an increase in the internal deformation of rocks is achieved, however, with only a small amount of volume loss, on the order of 5% of porosity at Sites 673 and 674 with respect to oceanic Site 672 (Wilkens et al., this volume). Moreover, the porosity-depth profile recorded at Site 673 in a single early Miocene siliceous clay interval does not show any significant divergence from an empirical curve describing normally compacting sedimentary columns, although the borehole crosses an overturned fold and out-of-sequence thrusts. Significant continuing progressive deformation of the sediments continued with modest water loss because of the low matrix permeability of the sequence (Taylor and Leonard, this volume).

The behavior of the sediments being underthrusted below the décollement is not so easy to assess. They do not show much macroscopic deformation, either in the cores (bedding dips remain low and the scaly fabric at Site 671 is restricted to a few tens of meters below the décollement), or on the seismic profiles (if we eccept normal faulting related to a Paleogene pre-subduction stage). Near to and a few tens of kilometers from the deformation front, seismic profiles show only a slight reduction in the thickness (in time) of the underthrust sequence that could be related to some compaction or a water-loss process (Westbrook et al., 1982; Ladd et al., and Screaton et al., this volume).

Close examination of physical properties (Wilkens et al., this volume), and of the clay mineralogy (Capet et al., Schoomaker Tribble, this volume) indicate subtle changes in sediments being underthrust. Of particular interest is the comparison between the Oligocene sections at Site 672, in the abyssal plain, and at Site 671, below the décollement. The most noticeable differences are (Fig. 5): (1) the higher delta porosity at Site 671 with

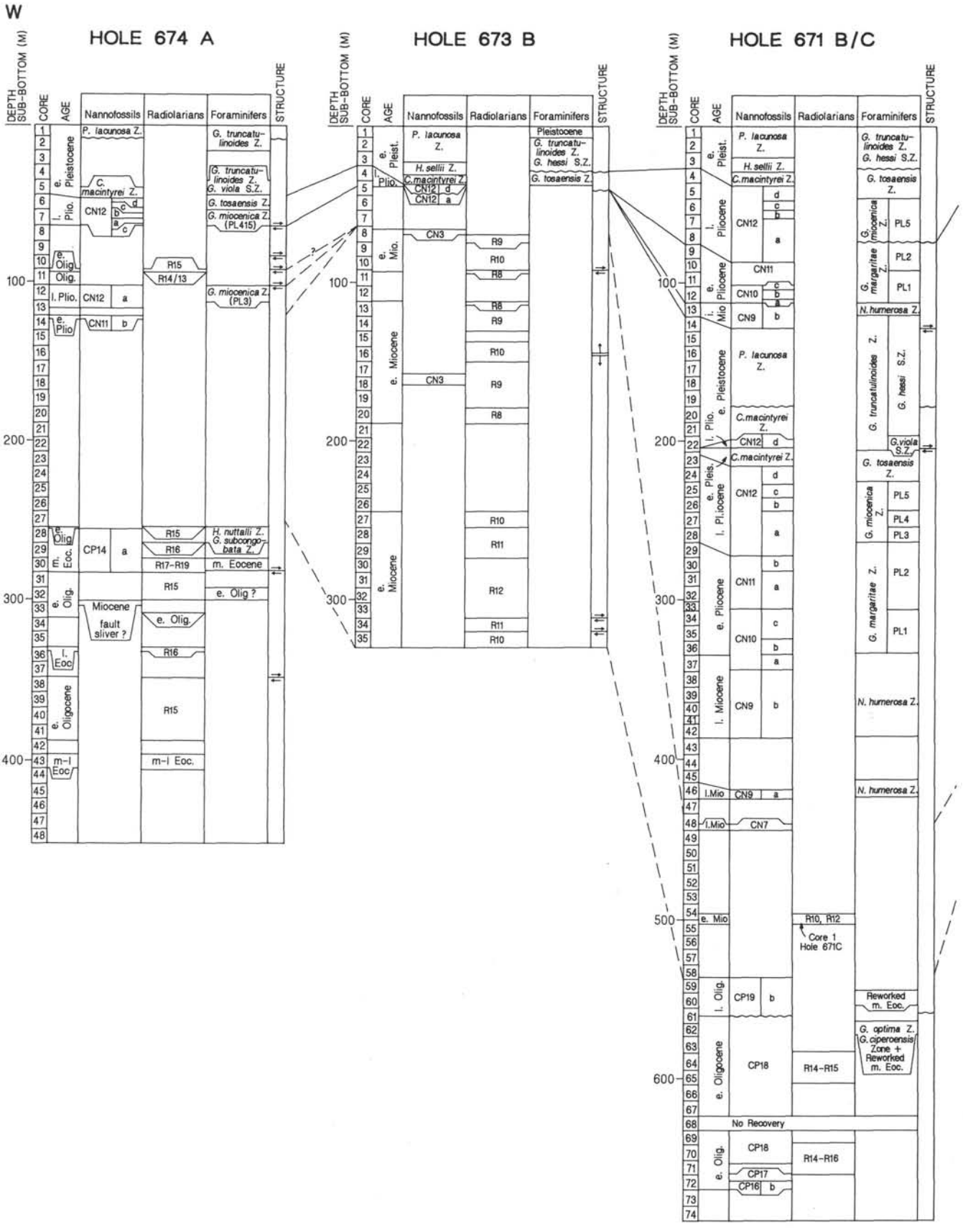

Figure 2. Biostratigraphic summary of Leg 110 Sites showing locations of biostratigraphically defined structural features (from Clark, cenozoic calcareous nannofossils, this volume). Diagonal age boundaries indicate areas of disagreement between nannofossils and foraminifers.

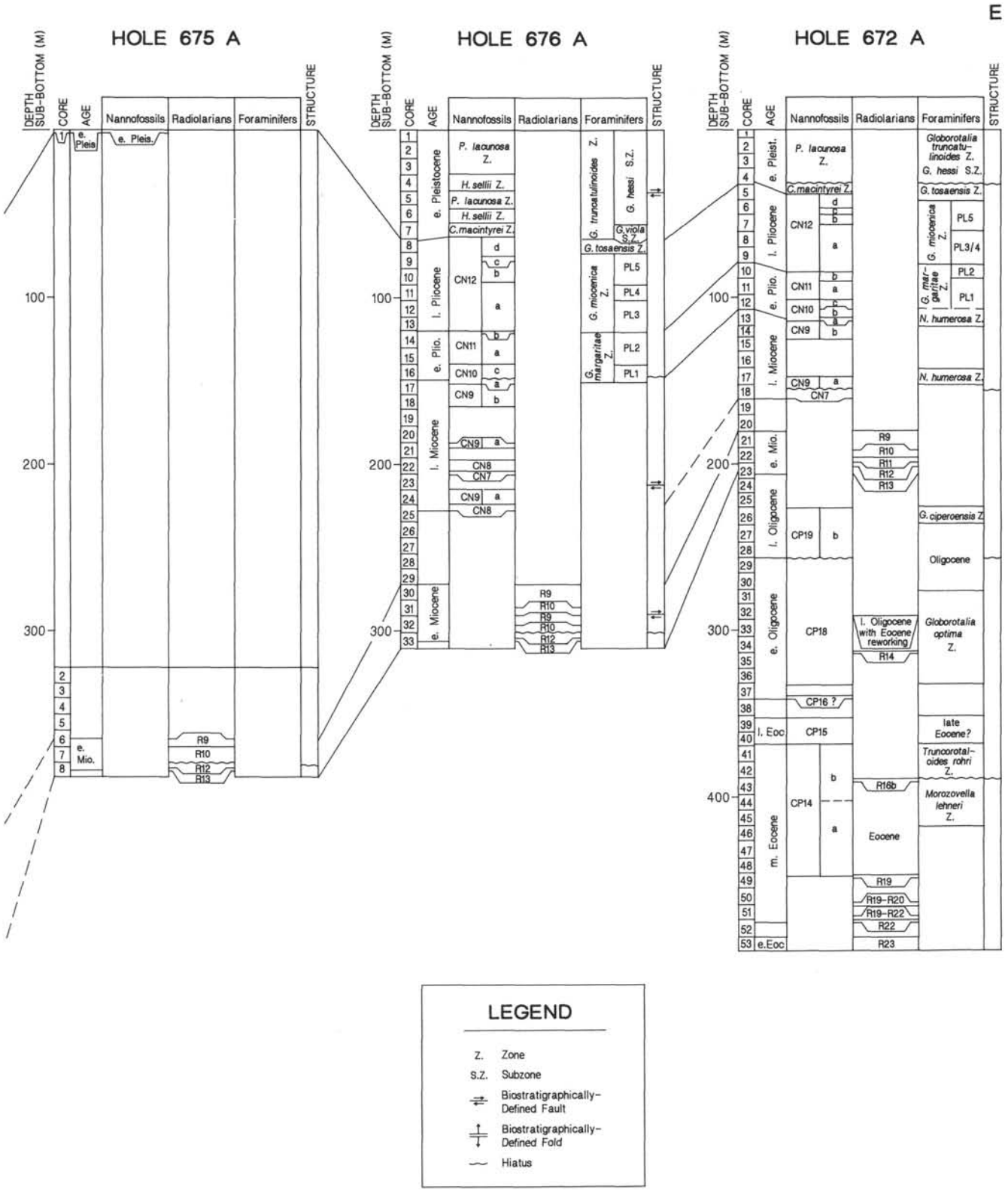

Figure 2 (continued).

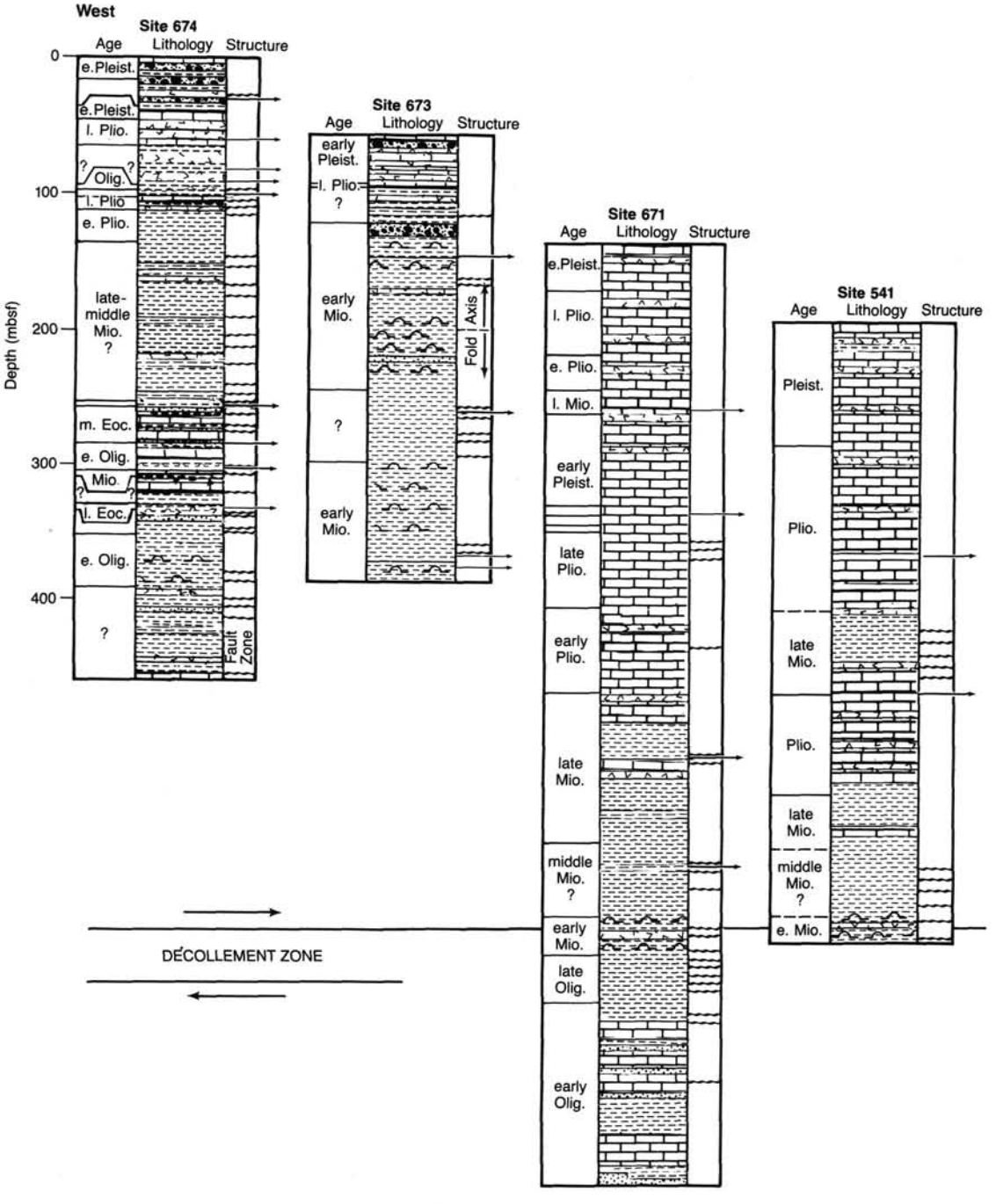

Figure 3. Stratigraphic summary of Leg 110 ODP and Leg 78A DSDP sites. Age boundaries taken from nannofossil biostratigraphy where disagreement exists. Faults include those defined by biostratigraphic data and structural features of cores.

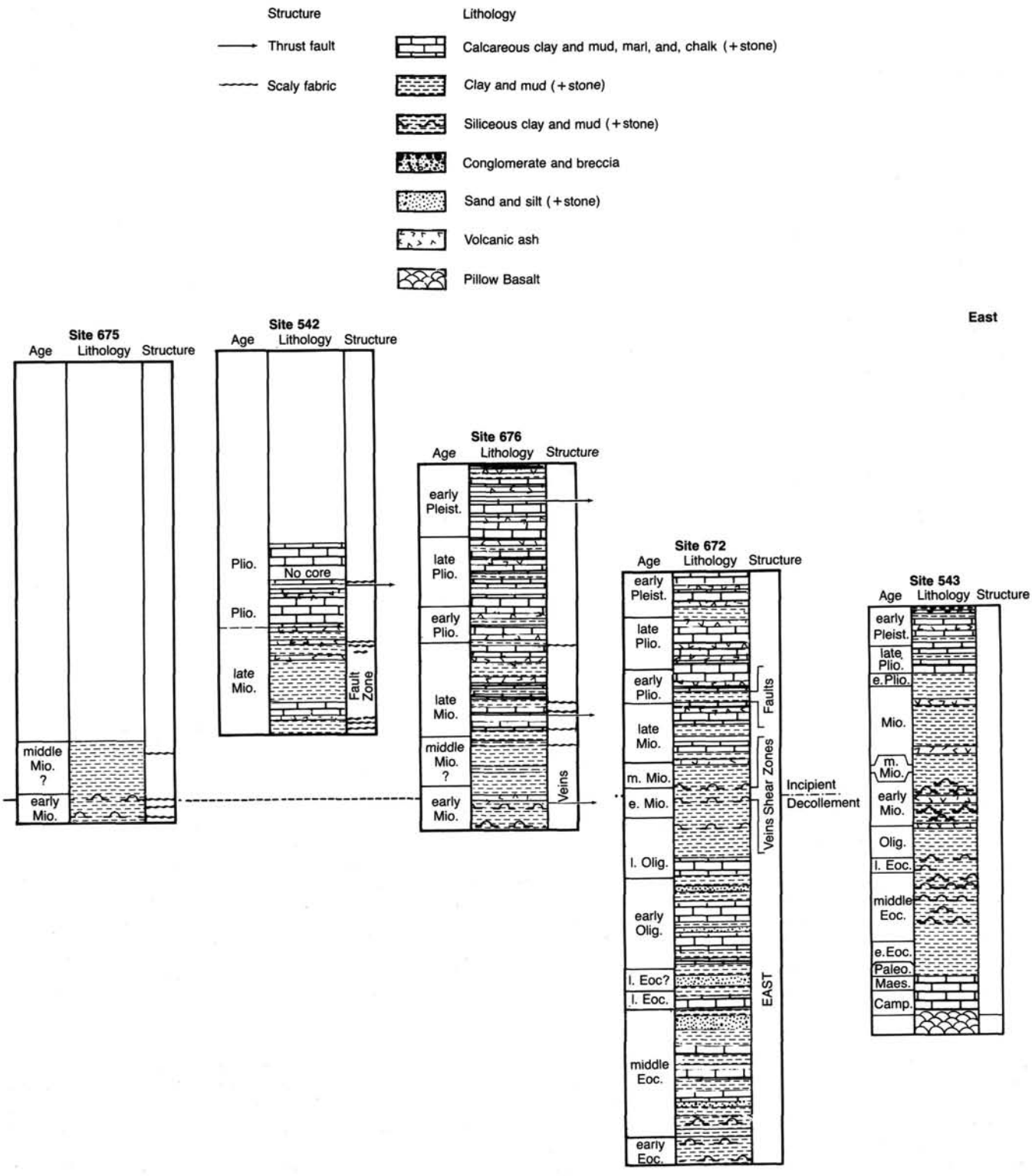

Figure 3 (continued).

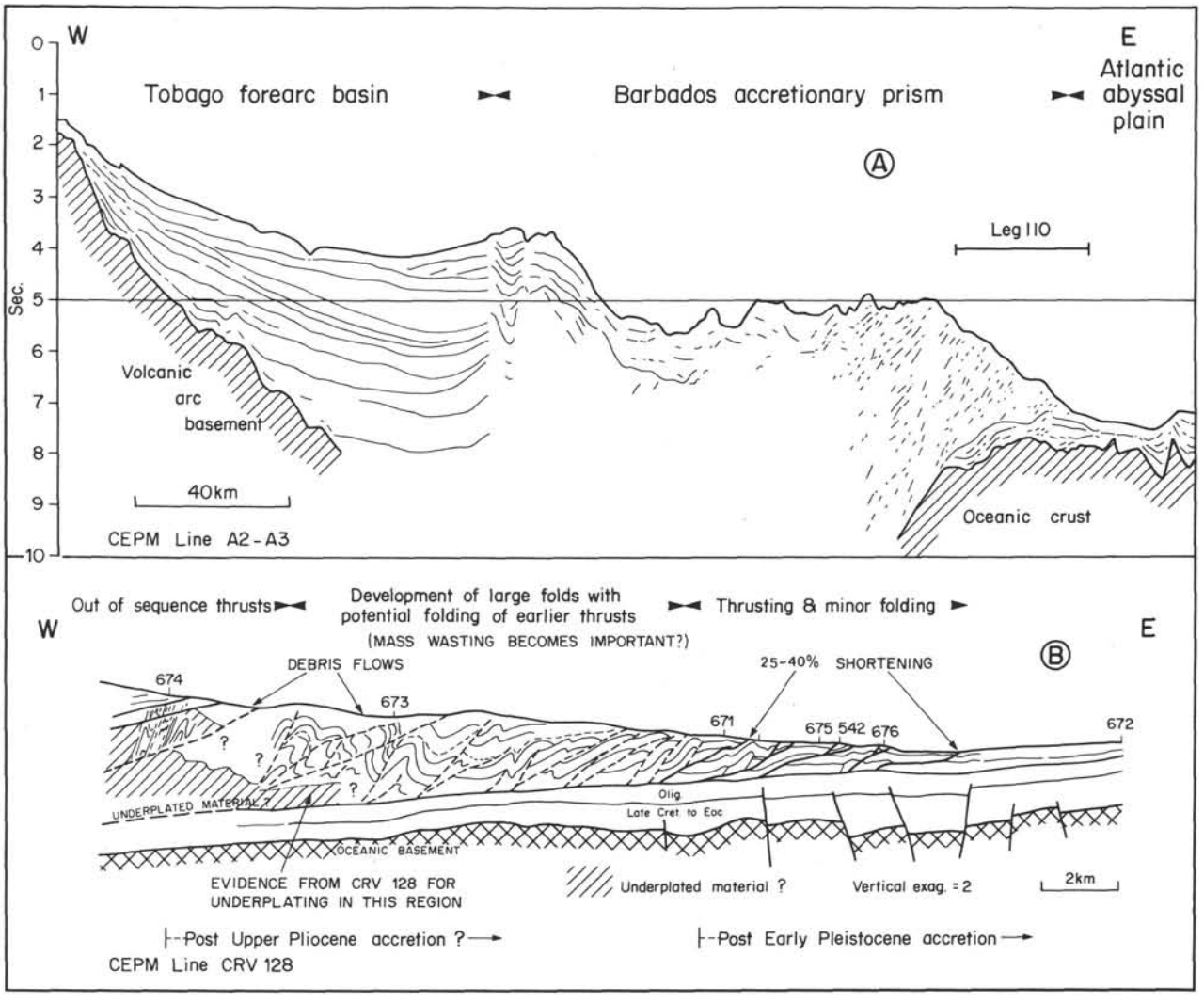

Figure 4. Tectonic features of the Northern Barbados Ridge. (A) Regional section showing, from east to west, (1) The Atlantic oceanic plain with a thin sedimentary cover of Senonian to Pleistocene age. Note the rough topography of the oceanic basement related to transform faults; (2) The Barbados accretionary complex. The rapid deepening to the west of the oceanic basement below the prism is directly related to the deepening of the basement south of the Tiburon Rise. There is also some suggestion from the seismic data that the décollement is deepening to the west from the early Miocene horizon to a layer closer to the basement; (3) The very thick Tobago forearc basin that is bounded to the east by active high-angle faults. The sedimentary infilling is onlapping the volcanic arc basement to the west. Location shown on Figure 1, back pocket. (B) Interpreted section across the entire length of the Leg 110 transect (from Brown et al., this volume). (C) Correlation of active faults from the seismic data, and pore-water anomalies at the toe of the accretionary complex from Site 676 (from Blanc et al., pers. commun.). The backthrusts west of Sites 672 and 542 are from high-resolution seismic data and S.A.R. imagery recently acquired by Lallemand, et al. (in press). (D) Fabric elements associated with the various structural environments at the toe of the prism: (a) mud-filled veins associated with incipient shears (Site 672); (b) compressive stresses initiating conjugate reverse faults that are confined to the off-scraped section above the décollement; (c) possible layer-parallel extension in response to the combined effects of vertical loading and simple shear immediatly beneath the décollement; (d) layer-parallel compression during later underplating of initially underthrust material; (e) flattening of fold in response to a sub-horizontal axis of compression with vertical extension (from Brown and Behrman, this volume).

respect to 672, suggesting that Oligocene strata are undercompacted at Site 671; (2) the decrease in relative smectite content at Site 671 and the correlative decrease in percentage of smectite interlayers with respect to Site 672, indicating some diagenetic alteration, possibly with the conversion of smectite to illite and the release of free water. Delta porosity is the difference between the porosity measured in the Leg 110 boreholes and that of an emperical standard terrigenous sediment compaction curve (Wilkens et al., this volume). The neoformation of illite could explain the decrease in crystallinity of this mineral observed from Site 672 to Site 671. The process by which the smectite is transformed to illite could involve the circulation of chemically reducing fluids in the décollement and below (Schoomaker Tribble, this volume), as supported by the presence of a large amount of dissolved manganese at the décollement level (G. Blanc et al., pers. commun.). The related release of water would favor the undercompaction of Oligocene strata below the décollement. Undercompaction of the Oligocene strata could also result from the underthrusting, consequent increase in vertical load, and insufficient time for consolidation.

Oligocene and Eocene rocks similar to those cored at Sites 671 and 672 were drilled at Site 674. Two hypotheses potentially explain their incorporation in the accretionary complex (Behrman et al., 1988). They could represent an older stage of frontal

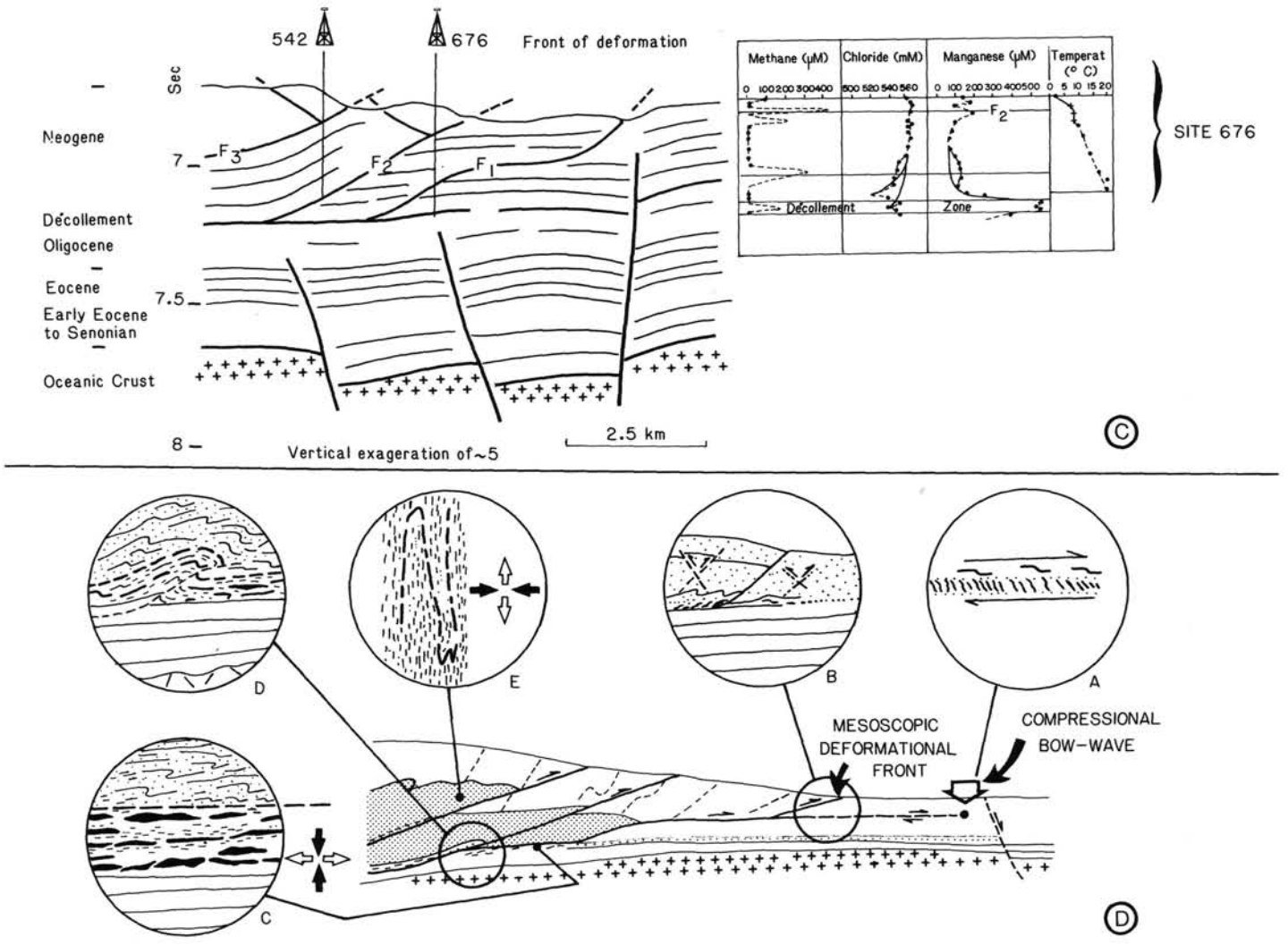

Figure 4 (continued).

accretion (in Miocene times for instance), when the décollement was at a deeper stratigraphic level than the present early Miocene one. Alternatively, they could represent underplated units related to any recent deepening of the décollement. In both cases their present location is related to recent uplifting along observed out-of-sequence thrusts (as also evidenced by their diagenetic index, Wilkens et al., this volume). There is currently no conclusive argument in favor of one or the other hypothesis from the cores or the seismic data. The Oligocene and Eocene rocks cored at Site 674 do not show the diagenetic changes in percent of smectite interlayers observed in the Oligocene underthrust series at Site 671, as should be expected in the second hypothesis. It has been argued, however (Brown et al., this volume), that a first phase of deformation observed at Site 674 and expressed by layer parallel extension and boudinage, might have occurred in the décollement zone after a substantial distance of underthrusting where tectonic loading could have promoted overpressuring and flattening strain. Extension of the underthrust sediments by pure shear is unlikely because these sediments are laterally constrained and can only consolidate vertically. Conversely, large extensional strains can be achieved in shear zones. Thus, passing of sediment through the décollement shear zone or any fault zone could cause the observed extensional deformation.

HYDROLOGIC SYNTHESIS

Sedimentary accretionary prisms consist of two hydrologic end members: (1) systems dominated by low permeability, fine-grained sediments, and (2) margins with abundant higher permeability sandy sediments. Faults dominated by fracture permeability are the initially dominant fluid expulsion conduits in systems characterized by low permeability, fine-grained sediments; systems with sandier sequences can, at least initially, dewater through stratigraphically controlled zones of high intergranular permeability. The northern Barbados Ridge in the Leg 110 area comprises a good example of an accretionary prism composed of low permeability sediments and is therefore useful in defining a hydrogeologic end member at convergent plate boundaries.

Definition of Fluid Flow Conduits and Apparent Timing of Flow

Pore-water chemistry and heat-flow data provided the best tools for defining the regions of active fluid flow, especially when considered in the context of structural data. Evaluation of pore-water anomalies from all sites reveal: (1) a region of methane-free fluids consisting of the accretionary prism, and (2) a realm of methane-bearing fluids, consisting of the décollement

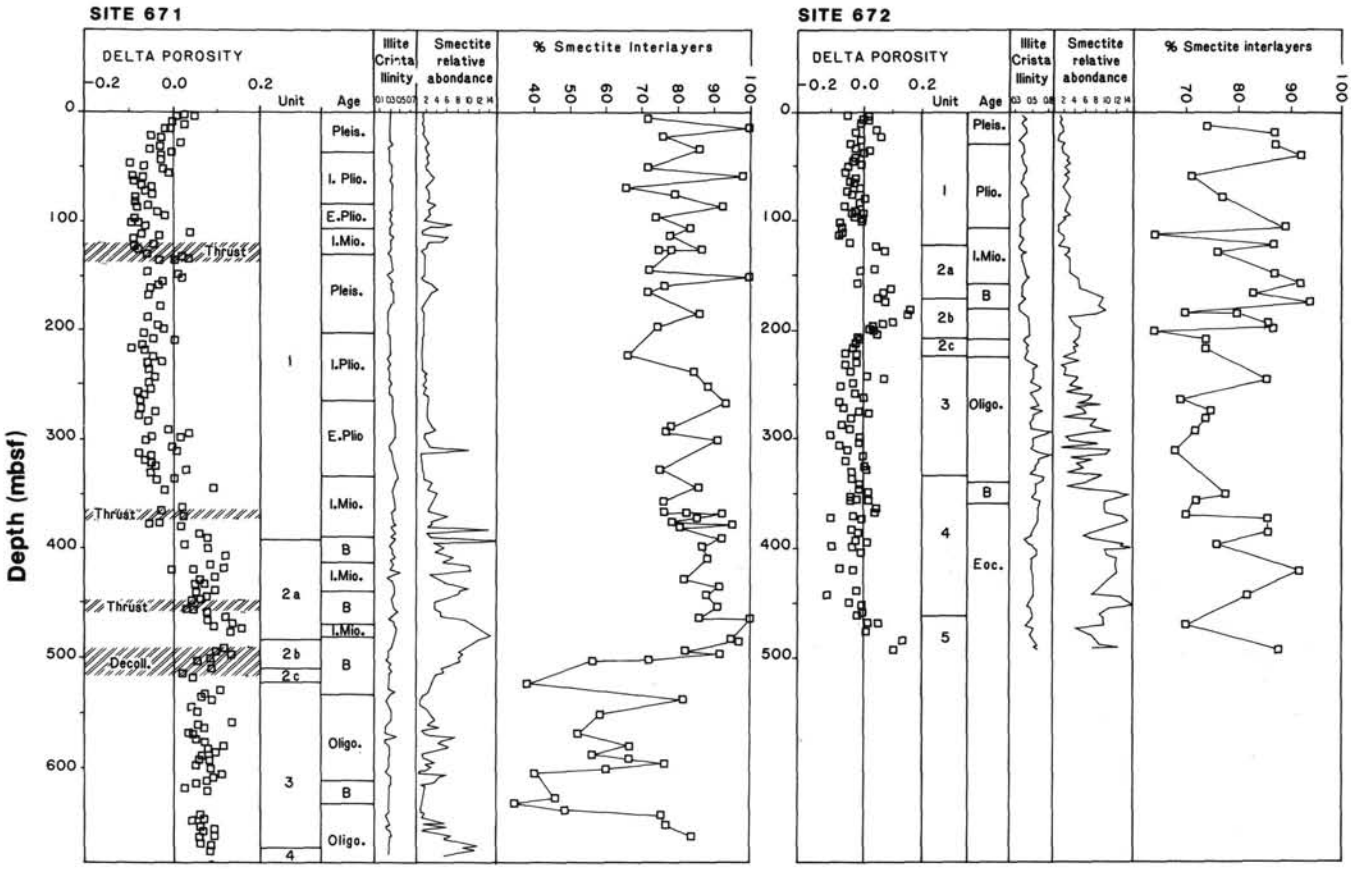

Figure 5. Comparison of the delta porosity, the illite cristallinity, the smectite relative abundance, and the percentage of smectite interlayers at Sites 671 and 672. Note the differences between the Oligocene series at the two sites, suggesting both overpressuring and clay diagenesis in the underthrust sequences. From Wilkens et al., Capet et al., Schoomaker Tribble, this volume.

zone and underthrust sediments (Gieskes et al., this volume; G. Blanc et al., pers. commun.; Fig. 6). Excepting the sandy layers in the underthrust sedimentary sequence, geochemical anomalies are universally associated with faults. Heat-flow profiles, available from Sites 672, 674, and 676, show changes in temperature gradients spanning faults that also are most readily explained by fluid flow along them (Fisher and Hounslow, this volume).

Both the thermal and geochemical anomalies observed in the drill cores would decay unless fluids are continually replenished. The thermal data provide the most critical measure of the rate of fluid flow, because temperature anomalies decay more rapidly than chemical anomalies. Heat-flow calculations suggest the episodicity of flow is in the range of tens to thousands of years (Fisher and Hounslow, this volume), which is consistent with the time interval of large earthquakes at subduction zones (Kanamori, 1972), and suggests a tie between deformation and fluid flow. Faults that do not show thermal anomalies but do have pore-water anomalies have probably experienced fluid flow in the past several hundred thousand years (J. Gieskes, pers. commun.). A critical unresolved question is the degree to which any episodic flow is superimposed on a lower rate of background flow.

Sources of Fluids and Distance of Transport

Porosity collapse during deformation can produce a substantial amount of fluid (Screaton et al., this volume), however geochemical signatures suggest involvement of mineral dehydration processes and hydrocarbon formation in fluid generation. The negative chloride anomalies and the positive methane anomalies are the two most striking geochemical features along conduits of fluid flow (Gieskes et al., this volume; G. Blanc et al., pers. commun.) and are indicative of fluid sources other than porosity collapse.

The negative chloride anomalies along faults are broadly associated with waters enriched in ^{18}O (Vrolijk et al., this volume). Fluids with these geochemical signatures could be explained by smectite dehydration because structurally bound water would be both fresher and presumably isotopically heavier than seawater (Vrolijk, this volume). However, detailed pore-water sampling of one core in the décollement zone shows a lack of correspondence between the chloride anomalies and the heavier oxygen values (Vrolijk, this volume). Apparently the combination of heavy oxygen and chloride anomalies are produced by more than just the process of smectite dehydration.

Smectite dehydration may be important in altering the composition of waters in the Leg 110 area because smectite constitutes about one-third of the total non-calcareous sediment in the Leg 110 area (Schoonmaker Tribble, this volume). Schoonmaker has calculated that complete conversion of smectite to illite in Leg 110 underthrust sediment would produce the observed freshening of the fluids in the décollement zone, if porosity was reduced sightly prior to conversion. Moreover, her data suggest that the incipient stages of the smectite-illite conversion are occurring in underthrust sediments beneath Site 671.

Because the concentrations of methane in fault zones and in the underthrust sandy horizon are very small, it is unlikely that hydrocarbon generation contributed much to the total fluid flux.

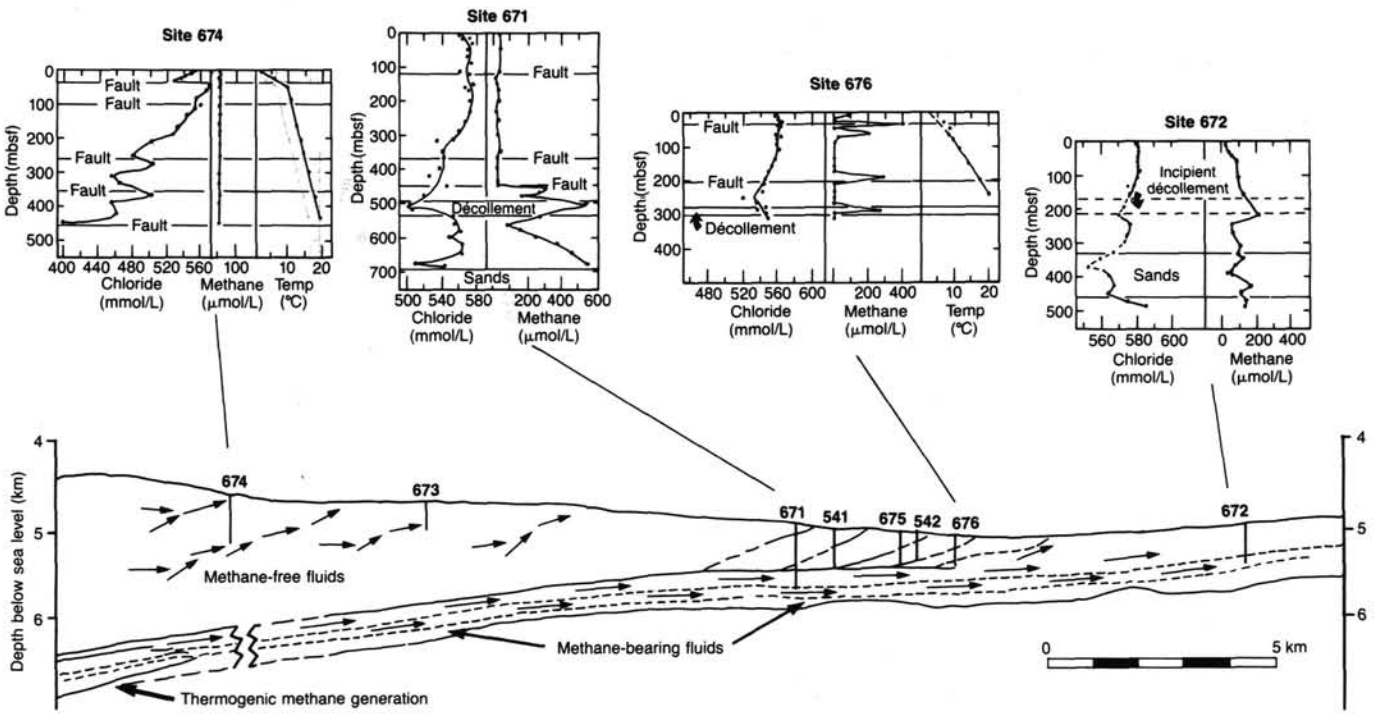

Figure 6. Plots of methane and chloride concentrations in pore waters, and temperature gradients from selected sites. Note that methane anomalies are restricted to intervals below the décollement zone defining a methane-bearing fluid realm. The virtual absence of methane in the accretionary prism defines the methane-free fluid realm. The thermogenic nature of the expulsed methane indicates derivation from east of the end of the cross section.

Nevertheless, the probable thermogenic nature of the methane (Vrolijk, this volume) suggests deep fluid sources with lateral flow of at least 50 km.

Physical Constraints on Fluid Flow

With the exception of the undeformed, underthrust sandy sequence, all evidence suggests that fluids flow preferentially along the décollement or related faults. Near the toe of the accretionary prism (arcward to Site 671), the sediments just above the décollement zone are of low-permeability material (Taylor and Leonard, this volume); hence, a fracture permeability associated with faulting would be a likely path for fluid loss (Fig. 7). At Site 674, sands equivalent to those now being underthrust are incorporated into the accretionary prism. This lithology did not show any geochemical or temperature anomaly indicative of rapid fluid flow, even though the sand remains permeable. Apparently the hydraulic continuity of the thin (<35 cm) sand beds has been broken by the deformation.

The contrast between the methane-bearing and methane-free fluids across the décollement zone (Fig. 6) is the most fundamental difference in fluid composition observed at the Leg 110 drill sites. The probable thermogenic origin of the methane beneath the décollement zone requires that the fluid be derived from a region at least 50 km arcward of the deformation front. The constraining of fluid flow beneath the accretionary prism for this distance requires that the hydraulic conductivity along the décollement zone be three to five orders of magnitude higher than the hydraulic conductivity through the base of the overlying accretionary prism (Wuthrich et al., this volume; Fig. 7).

The increased permeability along the décollement zone may result from: (1) permeability anisotropy due to the preferred orientation of fractures (Fig. 7), (2) permeability anisotropy resulting from orientation of phyllosilicates parallel to the décollement zone (Fig. 6), (3) low inclination of the maximum principal stress in the accretionary prism that would tend to prevent steep hydrofracturing (Fig. 6), or (4) a dynamic permeability as a result of deformational pumping along the décollement zone (Fig. 8).

Both a sub-planar shear fracture network characteristic of scaly foliation and sub-planar orientation of phyllosilicates that may be sub-parallel to the fractures strongly influence the tortuosity of fluid flow and therefore alter permeability directionally (Arch and Maltman, in press). According to Arch and Maltman, the permeability of experimentally produced shear zones in muds may be two to three orders of magnitude higher along rather than across the shear surface. This factor alone approachs the three to five orders of magnitude difference in permeability between the accretionary prism and the décollement zone suggested by the modeling of Wuthrich et al. (this volume).

The probable shallow inclination of the regional maximum principal stress in the Leg 110 area should cause the development of hydrofractures at acute angles to the décollement zone and therefore impede fluid flow at high angles to it. Although Coulomb failure surfaces would also form at low angles to the décollement zone, they would have a higher normal stress than any hydrofractures parallel to the maximum principal stress and therefore would be less readily useable as fluid flow conduits.

Deformational Pumping

An integrated evaluation of the heat-flow and pore-water chemistry data suggests that faults in the Leg 110 area have a history of variable fluid flow and probably variable fluid pressure. However, this probable episodic flow is likely to be superimposed on a constant background flow generated by regional hydraulic gradients. The apparent cyclicity of pressure and flow may be explained by a deformational pumping mechanism associated with incremental fault displacement (Fig. 8, Sibson et al. 1975; Sibson, 1981; Etheridge et al., 1984; Vrolijk 1987). Fault movement associated with deformational pumping would rely on a dynamic permeability higher than the static permeability

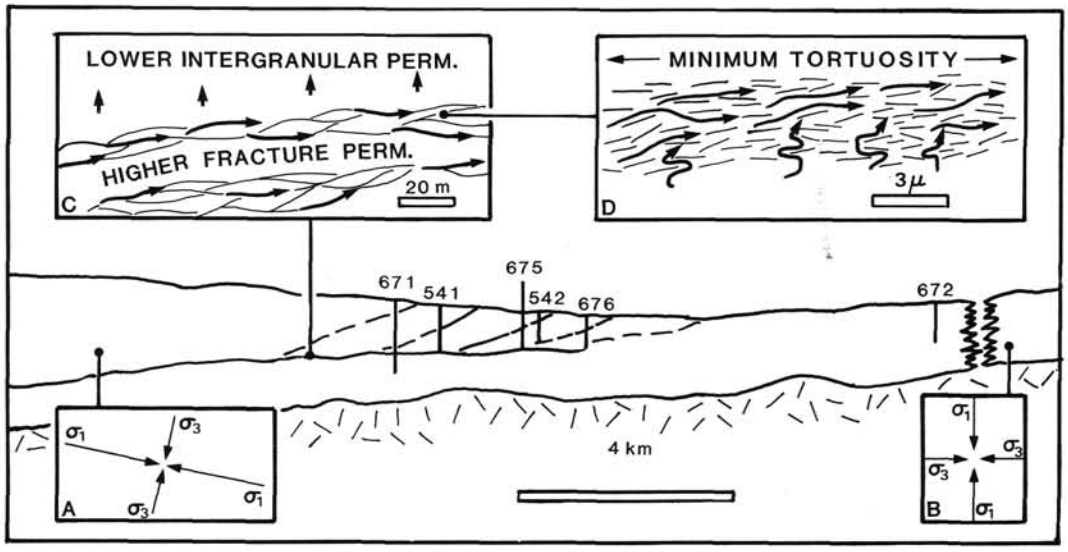

Figure 7. Detail of Leg 110 transect showing probable orientation of stress in prism, and schematic diagram of enhanced permeability in the décollement zone. Insets A and B illustrate state of stress in basin sediments and sediments of accretionary prism. This change in stress orientation occurs during underthrusting and perhaps with the transfer of sediments across the décollement zone. Inset C depicts the role of fracture permeability in providing substantially higher permeability along the décollement zone. Inset D shows how the orientation of mineral grains can provide a fabric of minimum tortuosity parallel to the décollement zone. A similar argument applies to the oriented fracture surfaces shown in inset *C*.

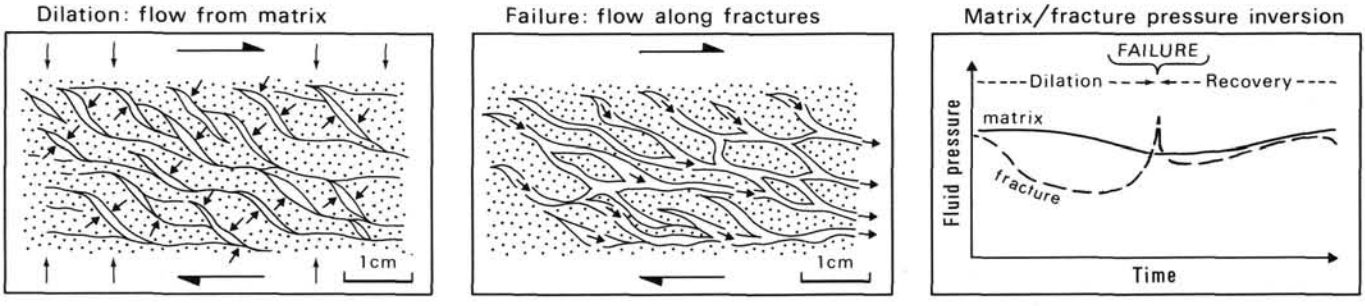

Figure 8. Deformational pumping. During initial deformation, fractures associated with scaly fabric in décollement zone dilate with flow from the matrix. With continuing deformation, fractures coalesce, resulting in failure. During failure the pressure in fractures exceeds that in the source matrix during collapse of dilatant fabric. Because of its low permeability, the matrix does not record this brief increase in pressure. During the "recovery" phase the matrix pore-fluid pressure returns to its pre-dilatant state, being replenished from far-field sources, and the deviatoric stress increases again, ultimately leading to a subsequent dilation and reinitiation of the deformational pumping cycle.

of the fault rocks and much higher than the permeability of the surrounding matrix. A scenario of coupled fluid flow and fault movement initially involves the dilation of scaly fabric with fluid flowing to zones of localized fluid pressure minimal within dilatant fractures. As the number of dilated fractures increases the weakened sediment fails, with the interconnected dilated fractures providing the easiest path of fluid escape. During failure, fluid pressure briefly approximates lithostatic with opening of, and fluid flow along, an interconnected network. Because the dynamic fracture permeability parallel to the décollement zone would be much higher than the matrix permeability of the sediment adjacent to the décollement zone, fluid cannot flow back to its source region and is pumped along the décollement zone.

Fluid Flow and Minimum Effective Stress in the Décollement Zone

The décollement zone is both a region of fluid expulsion and a failure surface. Extensive thrust surfaces are commonly thought to be characterized by high fluid pressures (e.g., Hubbert and Rubey, 1959); conversely, zones to which fluid flows, also the décollement in this case, are believed to be intervals of low fluid pressure. This apparent contradiction is resolved by considering fluid flow and faulting in terms of head and effective stress, respectively.

The pressure gradients illustrated in Figure 9 are derived by the modeling of Wutherich et al. (this volume), which are in turn based on the "inadvertent packer experiment" of Leg 78A (Biju-Duval, Moore et al., 1984). Each of these plots shows an inferred pressure vs. depth plot at Site 671 with its lateral extension toward a similar plot at Site 542. Head is the elevation to which water would rise in a manometer (pipe) inserted at any depth. For example, all points on the hydrostatic pressure gradient have the same head. Similarly, any surface parallel to the hydrostatic pressure gradient would have constant head. Clearly, fluid moving up or seaward along the pressure gradient below the décollement (bold line with arrows) is moving down-head and would have a flow pattern consistent with the observations.

Effective stress is defined as the difference between the total stress (lithostatic gradient in Fig. 9) and the fluid pressure at any

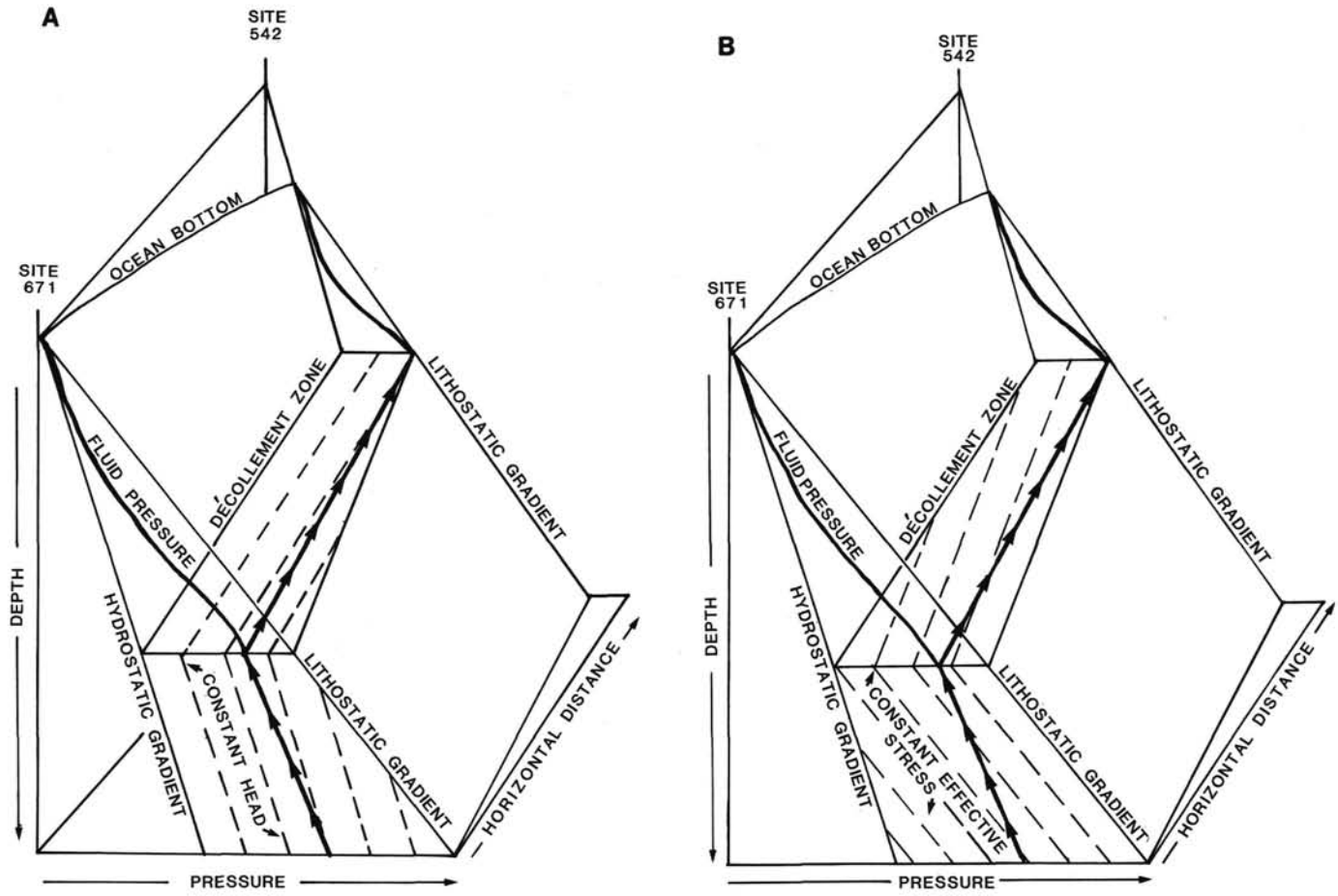

Figure 9. A. Plot of fluid pressure vs. depth vs. distance along Leg 110 transect, showing dashed surfaces of uniform head parallel to hydrostatic gradient. The bold line indicates fluid pressure distribution both vertically and horizontally. The arrows indicate fluid-flow vectors both within the underthrust sediments and along the décollement. Note that fluid always flows from regions of higher head to lower head. Fluid-pressure distributions constrained by "inadvertent packer experiment" (Biju-Duval, Moore, et al., 1984), and modeling of Wutherich et al., (this volume). B. Plot of fluid pressure vs. depth vs. distance along Leg 110 transect, showing surfaces of uniform effective stress parallel to lithostatic gradient. Fluid-pressure distribution and flow vectors are same as in A. Note that as fluid flows down head (as indicated in A it moves from a zone of higher effective stress (within the underthrusting sediments) to a region of lower effective stress (along the décollement zone). The effective stress also decreases toward the deformation front.

depth. The fluid pressure distribution on Figure 9b shows that the effective stress decreases to a minimum from the underthrust sediments up to the décollement and seaward from Site 671. For a material of uniform strength, failure is likely to occur under conditions of minimum effective stress, hence along the décollement zone.

The foregoing exercise demonstrates graphically and perhaps intuitively that, with a reasonable pressure gradient, the décollement zone can be both an interval that fluids can flow into and along which minimum effective stress may occur, and hence preferential failure. The assumption of uniform sediment strength is a conservative one because décollements commonly localize in weak sedimentary layers. The likelyhood of episodic flow (Fisher and Hounslow, this volume) and lower sediment strength (Wilkens et al., this volume) in the décollement zone would enhance the options for simultaneous deformation and flow along this major detachment.

Three-Dimensional Effects

Because the heat flow measured in the Leg 110 area is higher than that measured along-strike of the Barbados Ridge and because the Leg 110 area is located on a structural high with thin sediments, the Leg 110 area may focus fluid flow (Fisher and Hounslow, this volume). However, Fisher and Hounslow's comparisons are with areas to the south where the incoming sediment is more than three times thicker than that in the Leg 110 area (Speed, Westbrook, et al., 1984). This increased sediment thickness with hydraulic conductivity structure varying from that of the Leg 110 area might explain part of the differences in heat flow.

A critical question is how important are the three-dimensional effects in the Leg 110 area, especially in influencing flow along the décollement zone. If head is proportional to thickness of the accretionary prism overlying the déecollement (in accord with standard consolidation theory; e.g., Lambe and Whitman, 1969), and permeability of the underthrust sediments and décollement is uniform, then prism geometry can be used to evaluate hydraulic gradients. The rather uniform arcward thickening to the prism to the north of the Leg 110 area (Speed, Westbrook, et al., 1984) suggests that hydraulic gradients are maximized along a west-southwest direction sub-parallel to the Leg 110 transect; lateral flow into the Leg 110 area would be comparatively unimportant. Conversely to the south, the more rapid arcward thickening of the prism and the southeasterly trend of the deformation front (Speed, Westbrook, et al., 1984) suggests that maximum hydraulic gradients trend in a southwesterly di-

rection relative to the deformation front; accordingly, some southerly derived lateral flow into the Leg 110 transect may be possible.

CONCLUDING REMARKS AND SUGGESTIONS FOR FURTHER DRILLING

Because of its fundamental structural and hydrologic significance, penetration of the décollement zone was probably the single most significant achievement of Leg 110. Pore-water geochemistry coupled with temperature data and analyses of the cores and seismic data developed a framework for consideration of the effects of fluids on virtually every aspect of the geologic history of this margin. The drilling program clearly defined the conduits of flow but critical physical parameters remain unmeasured.

From the perspective of a land geologist, the upslope sites yielded some of the most significant results, with cores showing fabrics similar to those found in sub-aerially exposed melange terranes, yet still retaining 50% porosity. Similarly, the mechanism of transport and the regional correlation of the sands cored at Site 672 pose intriguing questions.

Because the northern Barbados Ridge is the only location where the décollement zone has been penetrated, the ridge provides exceptional opportunities for understanding this major feature. Further study of this surface might be best accomplished by drilling a series of holes through it to examine gradients in chemical, hydrogeologic, and geological parameters. A system of three holes, two located down-dip and a third alongstrike might most simply accomplish this goal. Any future drilling program, however, must be supported by reliable downhole instrumentation, including a packer, and allowing measurements of pore pressure, *in-situ* permeability, fluid-flow rate, and stress. Ultimately long-term monitoring will be necessary to evaluate the coupling of fluid flow and deformation; with monitoring, it may even be possible to relate these phenomena to the earthquake cycle.

The well-developed structural features in cores from the upslope sites of the Leg 110 transect deserve further exploration through several deep holes (1 km or greater) to investigate progressive structural evolution with depth.

ACKNOWLEDGMENTS

We thank the U.S. National Science Foundation and equivalent agencies in Canada, the European Science Foundation, the Federal Republic of Germany, France, Japan, and the United Kingdom for support of the Ocean Drilling Program. Moore acknowledges United States Science Advisory committee and the National Science Foundation (Grant OCE-869754) for support of data analysis and manuscript preparation. This report was improved by the comments of Shirley Dreiss, Roland von Huene, and Kevin Brown.

REFERENCES

Arch, J., and Maltman, A., in press. Anisotropic permeability and tortuosity in deformed wet sediment. *J. Geophys. Res.*

Baldwin, L. S., Harrison, T. M., and Burke, K., 1986. Fission track evidence for the source of accreted sandstones, Barbados. *Tectonics,* 5: 457–468.

Behrman, J. H., Brown, K., Moore, J. C., Mascle, A., and Taylor, E., 1988. Evolution of structures and fabrics in the Barbados Accretionary Prism: insights from Leg 110 of the Ocean Drilling Program. *J. Struct. Geol.,* 10:577–592.

Biju-Duval, B., Moore, J. C., et al., 1984. *Init. Repts. DSDP,* 78A: Washington, D.C. (U.S. Govt. Printing Office).

Brown, K. M., and Westbrook, G. K., 1987. The tectonic fabric of the Barbados Ridge accretionary complex. *Mar. Pet. Geol.,* 4:71–81.

Cello, G., and Nur, A., 1988. Emplacement of Foreland thrust systems. *Tectonics,* 7:261–271.

Etheridge, M. A., Wall, V. J., and Cox, S. F., 1984. High fluid pressures during regional metamorphism and deformation: implications for mass transport and deformation mechanisms. *J. Geophys. Res.,* 89: 4344–4358.

Hubbert, M. K., and Rubey, W. W., 1959. Role of fluid pressure in the mechanics of overthrust faulting. I: Mechanics of fluid-filled porous solids and its application to overthrust faulting. *Geol. Soc. Am. Bull.,* 70:15–166.

Kanamori, H., 1972. Tectonic implications of the 1944 and 1946 Tonankai and Nankaido earthquakes. *Phys. Earth Planet. Inter.,* 5:129–139.

Lambe, T. W., and Whitman, R. V., 1969. *Soil Mechanics:* New York (Wiley).

Lallemand, S., Henry, P., Foucher, J. P., and Le Pinchon, X., in press. Detailed structure and possible fluid pass at the toe of the Barbados accrectionary wedge—results of a deep-tow side-scan sonar survey. *Geology.*

Latouche, C., Maillet, N., 1984. Evolution of Cenozoic clay assemblages in the Barbados Ridge (Deep Sea Drilling Project Sites 541, 542, 543). *In* Biju-Duval, B., Moore, J. C., et al., *Init. Repts. DSDP,* 78A: Washington (U.S. Govt. Printing Office), 343–356.

Mascle, A., Moore, J. C., et al., 1988. *Proc. ODP, Init. Repts.,* 110: College Station, TX (Ocean Drilling Program).

Moore, J. C., Mascle, A., Taylor, E., Andreieff, P., Alvarez, F., Barnes, R., Beck, C., Behrmann, J., Blanc, G., Brown, K., Clark, M., Dolan, J., Fisher, A., Gieskes, J., Hounslow, M., McLellan, P., Moran, K., Ogawa, Y., Sakai, T., Schoonmaker, J., Vrolijk, P., Wilkens, R., and Williams, C., 1988. Tectonics and hydrogeology of the northern Barbados Ridge: results form Ocean Drilling Program Leg 110: *Geol. Soc. Am. Bull.,* 100:1578–1593.

Pudsey, C. J., and Reading, H. G., 1982. Sedimentology and structure of the Scotland Group, Barbados. *In* Leggett, J. K. (Ed.), *Trench-Forearc Geology:* Geol. Soc. Am. Spec. Publ., 10:291–308.

Sibson, R. H., 1981. Fluid flow accompanying faulting: field evidence and models. *In* Simpson, D. W., and Richards, P. G. (Eds.), *Earthquake Prediction: An International Review.* Am. Geophys. Union, Maurice Ewing Ser., 4:593–603.

Sibson, R. H., Moore J. McM., and Rankin, A. H., 1975. Seismic pumping—a hydrothermal fluid transport mechanism. *J. Geol. Soc. London,* 131:653–659.

Speed, R. C., 1983. Structure of the accretionary complex of Barbados, 1: Chalky Mount. *Geol. Soc. Am. Bull.,* 94:92–116.

Speed, R., Westbrook, G. Mascle, A., Biju-Duval, B., Ladd, J., Saunders, J., Stein, S., Schoonmaker, J., and Moore, J., 1984. Lesser Antilles Arc and adjacent terranes. Ocean Margin Drilling Program, *Regional Atlas Series, Atlas 10.* Woods Hole, MA (Marine Science International).

Stein, S., De Mets, C., Gordon, R. G., Brodholt, J., Argus, D., Engeln, J. F., Lundgred, P., Stein, C., Weins, D. A., and Woods, D.F.A., 1988. A test of alternative Caribbean plate relative motion models: *J. Geophys. Res.,* 93:3041–3050.

Vrolijk, P. J., 1987. Tectonically-driven fluid flow in the Kodiak accretionary complex, Alaska. *Geology,* 15:466–469.

Westbrook, G. K., Smith, M. J., Peacock, J. H., and Poultier, M. J., 1982. Extensive underthrusting of undeformed sediment beneath the accretionary complex of the Lesser Antilles subduction zone. *Nature,* 300:625–628.

Date of initial receipt: 2 March 1989
Date of acceptance: 1 May 1989
Ms 110B-158